Report "Photometric modelling & analysis of (859) Bouzaréah astreoid", academic year 2025/2026

As a part of passing the monograph "Physics of Asteroids", lecturer Prof. A. Marciniak

Oleh Ryzhov (II rok II stopnia, Astronomia)
Uniwersytet Adama Mickiewicza w Poznaniu

Abstract

Asteroids play a vital role in understanding the formation and evolution of our Solar System. One of the most basic, though the most important part of their analysis is photometric observations from ground-based observatories, and their processing to acquire the most basic parameters of an asteroid. In this report, we perform the analysis of 49 photometric observations of the main-belt asteroid (859) Bouzaréah for the last decade. We acquire the axis rotation period and provide insights towards the likely form of an asteroid, using the **convexinv** software, as well as the private or modified software by Prof. Marciniak and her team.

1 Introduction

The main-belt asteroid (859) Bouzaréah is a notable primitive body situated in the outer regions of the asteroid belt, with an orbital semi-major axis of approximately 3.23 AU, classified as an X-type object in the asteroid taxonomy type scheme (Tholen, 1984; Bus & Binzel, 2002; Vereš et al., 2015). The physical size of it is estimated to be set between 65 and 86 km (Ryan & Woodward, 2010; Masiero et al., 2012), with the uncertainty weighted mean value of 70.28 ± 0.39 (Choukroun et al., 2025). The most recent Convex Inversion Thermophysical Modelling, performed by Choukroun et al. (2025) suggests the size to be bound between 64 and 80 km, confirming the previous results, as well as suggesting the period of 24.9287 hours, and rotation axis to be positioned at $\lambda = 29°$ and $\beta = -45°$, or $\lambda = 220°$ and $\beta = -32°$. Two solutions for (λ, β) are connected to the polar disentanglement problem. The synodic period, indicated by previous studies is 23.2 hours[1].

2 Data

We have been extensively working with the .ATL file containing 49 series of photometric observations for the asteroid 859 Bouzaréah, collected between 2015 and 2023. These observations cover the number of positions of (859) on its orbit (see Figure 1), coming from the observational sites in Poland (Borowiec), Ukraine (Derenivka), the US (Winer Observatory; Lovell Observatory; Mt. Lemmon Observatory), Chile (TRAPPIST-S, La Silla Observatory), Lithuania (Moletai), the UK (Maindenhead), Turkey (Adiyaman), South Korea (SOAO), Spain (e-EYE), Hungary (Piszkéstető). All the observations provided are not reduced to absolute magnitudes (*REDUCED MAG is set to F[alse]*), though are sensitive-corrected and filter-corrected (*RELATIVE PHOT. is set to T[rue]*). No available TESS or Kepler data for the following asteroid was found, hence, was not included in the analysis.

3 Methods

The main physical idea of the methods used in this work is based on the asteroid photometric observations from different angles, i.e., at different relative positions to the Sun and to the Earth (observer). **Convexinv** software, written in Fortran by Mikko Kaasalainen, and converted to C by Josef Durech, computes the shape+spin+scattering models from the collected lightcurves, resulting not only in properties of rotation and

[1] https://www.astro.unige.ch/~behrend/page3cou.html#000859

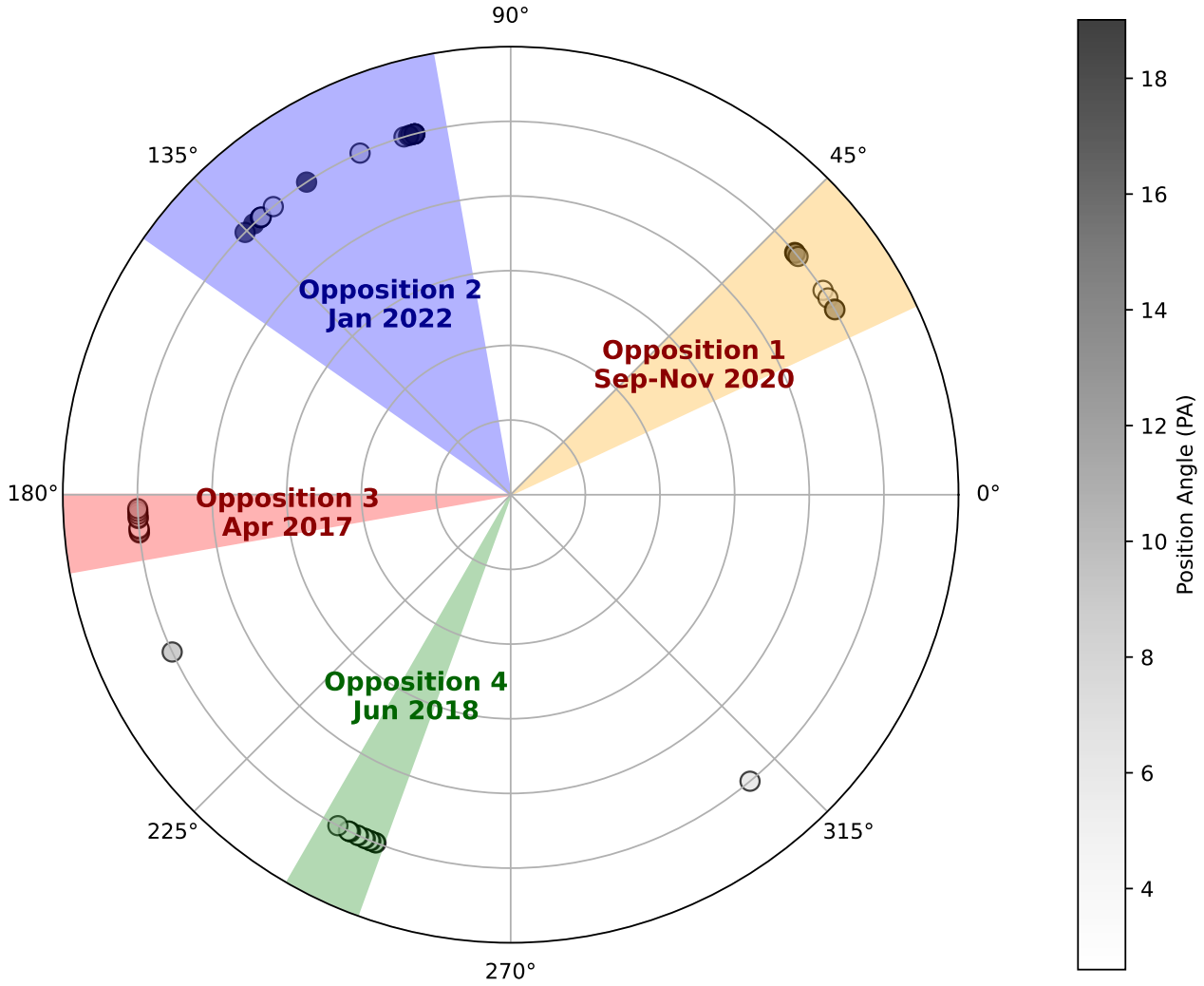

Figure 1: Polar plot of ecliptic longitudes of the 46 photometric observations, collected for (856). The colour of the points is determined by the Position Angle (PA) value, with the colour axis located on the right. The four distinct groups (oppositions) of asteroid positions are shown and highlighted with the shaded area. The time period of the majority of observations in each opposition labels the areas.

axis position, but also in the shape model, produced as the polyhedron, being the solution of the Minkowski procedure (Kaasalainen & Torppa, 2001; Kaasalainen et al., 2001). The **convexinv** works by applying the inverse lightcurve technique, i.e., by simulating the shape of the asteroid and creating several synthetic lightcurves, the software finds the closest solution to the observed lightcurves.

Before the **convexinv**, we use several other packages, i.e., *kad_pad* package developed to estimate the synodical period from the lightcurves of the singular opposition, and finally produces the magnitude-phase plots. Next, we use the *period_scan* code, in order to accurately acquire the synodical period by χ^2 analysis of the array of assumed periods.

4 Results

4.1 Opposition analysis

As previously mentioned, Figure 1 shows the distribution of the asteroid positions when it was observed. We can easily distinguish four distinct groups of observations: Opposition 1 (O1; ecliptic longtitude $\lambda \sim 40°$), Opposition 2 (O2; $\lambda \sim 100°$), Opposition 3 (O3; $\lambda \sim 180°$), and Opposition 4 (O4; $\lambda \sim 240°$). While the axis of "daily" rotation of the asteroid remains almost unchanged within couple of years, we would expect to see different rotation schemes in different oppositions caused by different angles between the light-of-sight from the Earth, and the rotation axis orientation. Thus, we group observations with similar λ, and perform *kat_pad* routine on them, assuming the search limit of period to be within 23.15 and 23.25 hours.

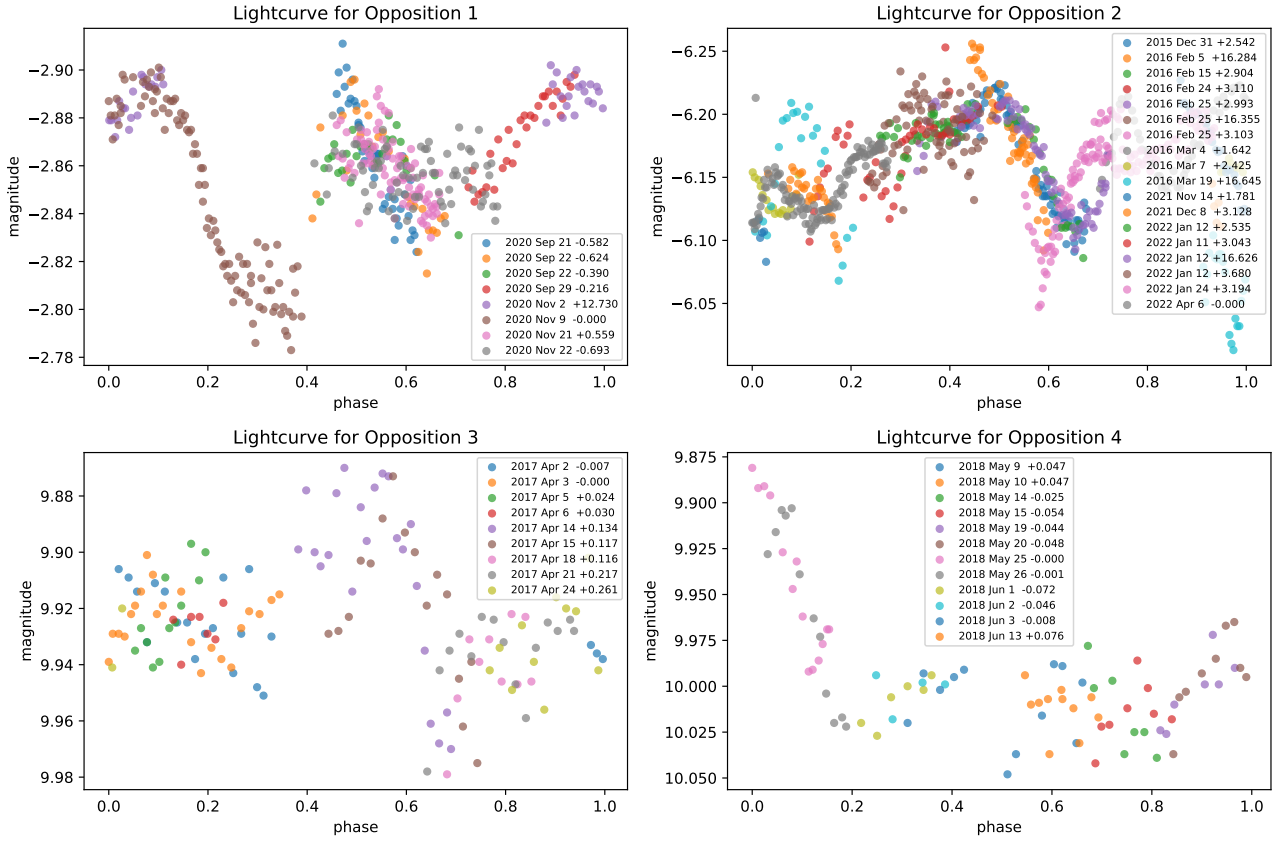

Figure 2: Four panels, showing the lightcurves, i.e., magnitude vs. phase plots, acquired for the 4 defined oppositions, mentioned in the title for each panel (see Fig. 1). The legend describes the date of the observations, marked as points of the corresponding point, with the correction relative to the zero time in the end of the line. Lightcurves were generated by the *kat_pad* software, and were not changed, shifted or reduced further.

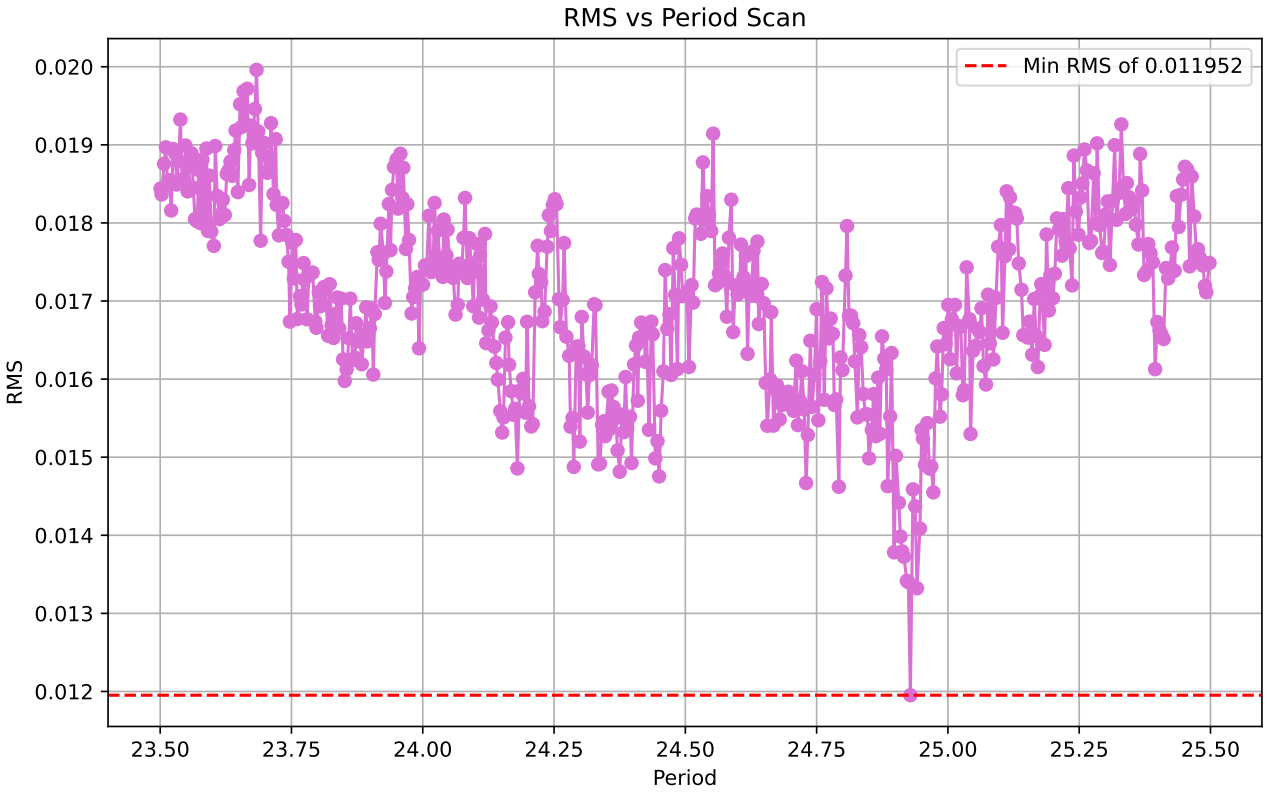

Figure 3: The Root Mean Square (RMS) vs. the assumed sidereal period. The red dashed line indicates the minimum value (also stated in the legend), while purple points represent the output of the *period_scan* code.

The results of *kat_pad* routine are shown in Figure 2. As can be seen, the asteroid's rotation changes drastically, e.g., in O3 and O4 the amplitude of the lightcurve (i.e. the range between minimum and maximum magnitude) is on the level of $0.02-0.05^m$, while in O1 and O2 on the level of $0.1-0.15^m$, not even mentioning the changes in shape of the lightcurve. Notably, all four panels contain either a visible lack of points, questioning the plots and derived periods, despite the narrow search range; or contain the suspicious scatters and unexpected bumps, e.g. the area of $0.6 - 0.8$ at the O1 panel. The fitted synodical period for all four oppositions stayed within $23.16 - 23.2$ hours.

4.2 Sidereal period estimation

One of the middle steps, before we started dealing with **convexinv**, is running the *period_scan* routine, which is aimed towards estimating the sidereal period of the axis rotation of the asteroid, which then would be used as the initial period value for the extensive **convexinv** modelling. Taking the sidereal period from the literature (e.g., Choukroun et al., 2025), and setting the range of $\sim \pm 0.5$ hour, we received the following array of periods, together with their Root Mean Square (RMS), presented at the Figure 3. The minimum RMS value corresponds to $P_* = 24.9285$, completely in alignment with (24.9287 ± 0.0003 Choukroun et al., 2025).

4.3 Positioning of rotation axis

Next, we switched to **convexinv** software, where we released both λ, β, as well as period P_*. To test as many possible rotation axs position, we have generated the grid of models, where the initial values of λ and β were pair combinations of $(0, 45, 90, 135, 180, 225, 270, 315)$ and $(-60, -30, 0, 30, 60)$ correspondingly, and period was set to the value we found in Section 4.2. All these combinations were applied to the **convexinv** routine, and resulted in 40 models tested, and two of those possessing the lowest χ^2 compared to the observed data. The grid showing the relation between acquired χ^2, and initial parameters is shown in Figure 4.

Figure 4 als contains two solutions with the lowest χ^2, i.e., S1 $(\lambda, \beta) = (36.199822, -45.167836)$; S2 $(\lambda, \beta) = (180.553893, -34.747492)$.

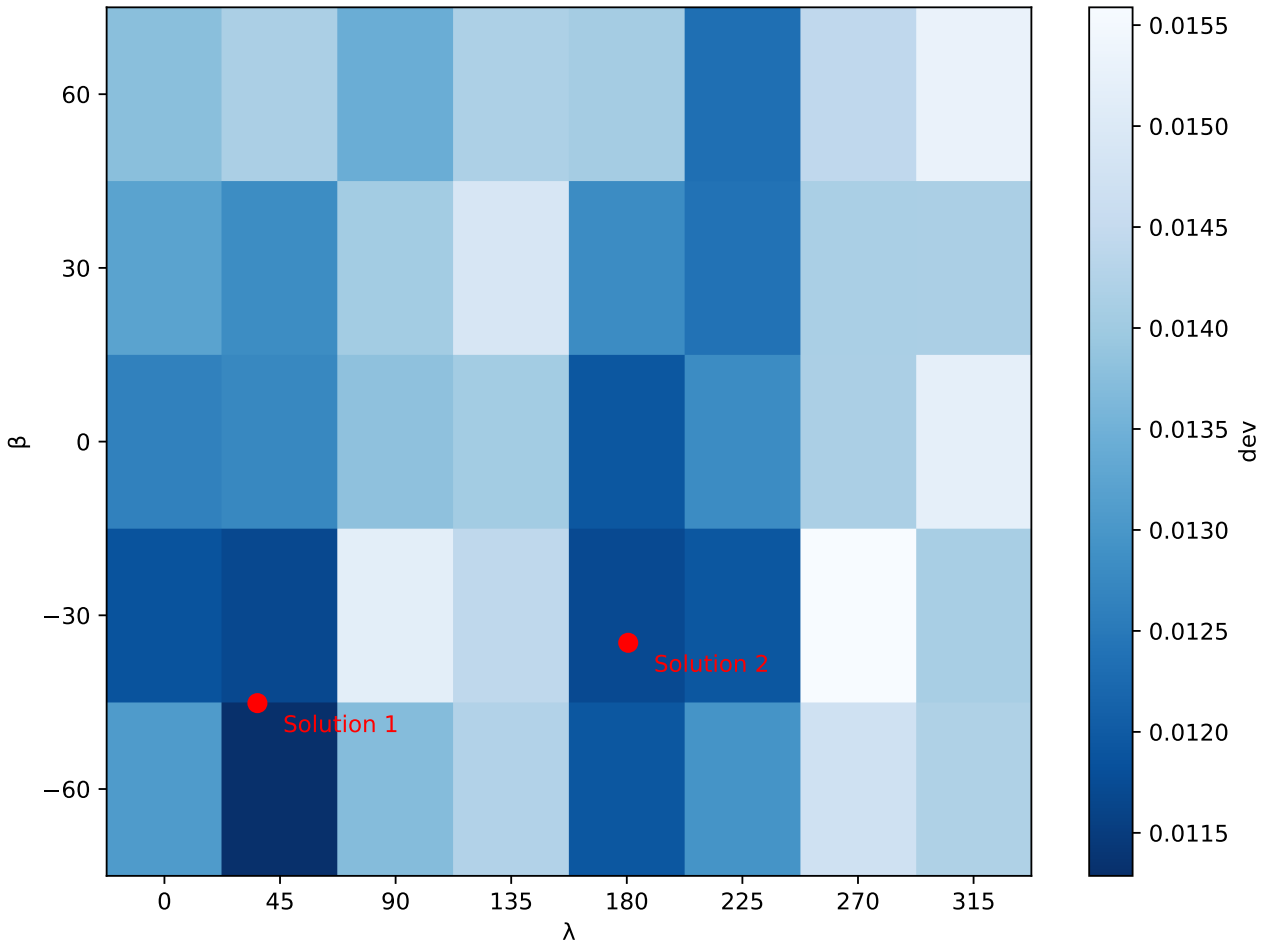

Figure 4: The RMS grid of the models, y-axis represents the initial assumed value for β, while x-axis displays the value for λ. The RMS value for the corresponding pair of (λ, β) is placed in the cross-section cell, and coloured according to the colourbar in the right part of the Figure. Two solutions with the lowest RMS are shown, as red points.

4.4 Shape of (859) Bouzareah

The huge advantage of **convexinv** code is that both S1 and S2 instantly have their shape representation, as well as the synthetic curve comparison with the observed, all accessed through the MATLAB routine. The Figures are presented in the Appendix, while in this Section we concentrate on their interpretation.

While all four generated 3D shape models look pretty similar, and can hardly be commented on or described, the panels containing the observed and synthetic curves sometimes indicate quite significant discrepancies between models and observations.

5 Discussion & Conclusions

In all previous Sections we have done the full photometric analysis of the lightcurves in .ATL format, acquired for almost a decade of observations worldwide of (859) Bouzareah asteroid. Our analysis contained the opposition identification (Fig. 1) and lightcurve presentation for each of the oppositions (Fig. 2), then the sidereal period estimation (Fig. 3), and then the model grid generation, and choosing the two best solutions (Fig. 4).

We will not go deeply into science, as it is a report; however, it is important to note several facts and their interpretation:

1. Strange bumps and chaos at Opposition lightcurves might indicate poor data quality, as well as might serve as a sign of the inaccurate assumption on the synodical period coming from the literature, which stays in place, according to the comments to the database with lightcurves[2]. However, the O3 and O4 clearly show that the asteroid does not change the crosssection significatnly, which might account for the low light curve amplitude, and O1 and O2 are already at the edge-on regime with the significant changes in cross-section, and hence, in brightness. This is also surprising, as usually we expect the asteroid to have a similar lightcurves in the opposite positions regarding Earth, if the rotation axis pole is located close to the ecliptic ($\beta \sim \pm 30^{\circ}$).

   However, such behaviour might not be artefact coming from the observations or analysis, but might also be caused by physics, e.g., the bimodality, disturbed rotation, shadow effect, etc. We leave the determination of the exact scenario to further observations and experts.

2. Determined sidereal period aligns well with the most recent findings of (Choukroun et al., 2025), which we suspect to be the statistical effect, coming from the fact that by 99% similar observations were used both in our work, and in Choukroun et al. (2025). However, the methodology of the two works is different, as here we applied the inverse composite modelling technique, while Choukroun et al. (2025) applied the Convex Inversion Thermophysical Model. In addition to that, the two solutions of both codes for the rotation axis coordinates are consistent with each other, but not the same: in our case S1 $(\lambda, \beta) = (36.199822, -45.167836)$; S2 $(\lambda, \beta) = (180.553893, -34.747492)$, while Choukroun et al. (2025) has S1 $(\lambda, \beta) = (29^{+24}_{-12}, 45^{+20}_{-17})$; S2 $(\lambda, \beta) = (200^{+24}_{-21}, 32^{+4}_{-30})$. This is, indeed, a reassuring finding, though still, might be biased due to the similar datasets used.

3. The comparison between observed and synthetic lightcurves for both S1 and S2 indicates the incompleteness of the model. Even though the uncertainties of observations were not given to us in the original .ATL file, and hence it is almost impossible to compare the deviation ($\sim 0.05^m$) with the typical photometric accuracy, but the large segments, where the offsets are either all positive or negative, definitely require addressing with better and more accurate models, which in their turn require already scientific expertise and effort.

Nevertheless, in this work, we have processed the large photometric observations of (859), determined its period, spin axis, and finally, the simple model of its shape, and gained practical experience with the codes, essential for better understanding asteroid physics.

References

Bus, S. J., & Binzel, R. P. 2002, , 158, 146, doi: 10.1006/icar.2002.6856

[2] https://www.astro.unige.ch/~behrend/page3cou.html#000859

Choukroun, A., Marciniak, A., Ďurech, J., et al. 2025, , 698, A298, doi: 10.1051/0004-6361/202554476

Kaasalainen, M., & Torppa, J. 2001, , 153, 24, doi: 10.1006/icar.2001.6673

Kaasalainen, M., Torppa, J., & Muinonen, K. 2001, , 153, 37, doi: 10.1006/icar.2001.6674

Masiero, J. R., Mainzer, A. K., Grav, T., et al. 2012, , 759, L8, doi: 10.1088/2041-8205/759/1/L8

Ryan, E. L., & Woodward, C. E. 2010, , 140, 933, doi: 10.1088/0004-6256/140/4/933

Tholen, D. J. 1984, PhD thesis, University of Arizona

Vereš, P., Jedicke, R., Fitzsimmons, A., et al. 2015, , 261, 34, doi: 10.1016/j.icarus.2015.08.007

6 Appendix

Below, you may find two sets of figures. First set is polyhedron models of asteroid, suggested by the **convexinv** software, where the asteroid's projections from the pole of X, Y, and Z axes are shown, from left to right panel. Asteroid rotates by default around Z-axis, thus the right shape represents the face-on shape, while the central and left show the asteroid from its edges. Asteroid shapes type 1 and type 2 do not differ much, but both are kept for fulliness of analysis.

Another set of figures are comparison between observed (blue points), and synthetic lightcurves (red lines), for all 49 series of observations.

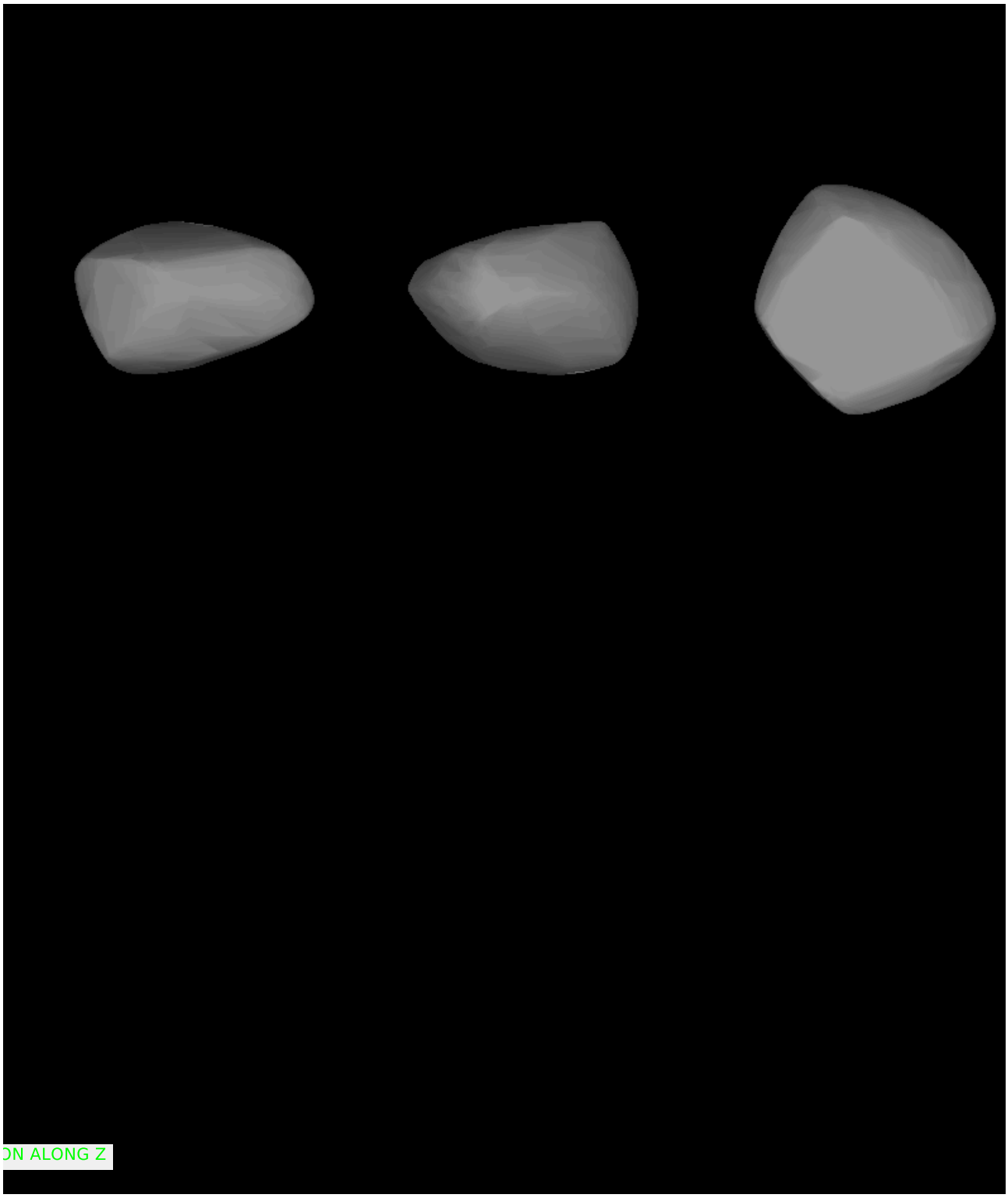

Figure 5: S1. Asteroid shape 1.

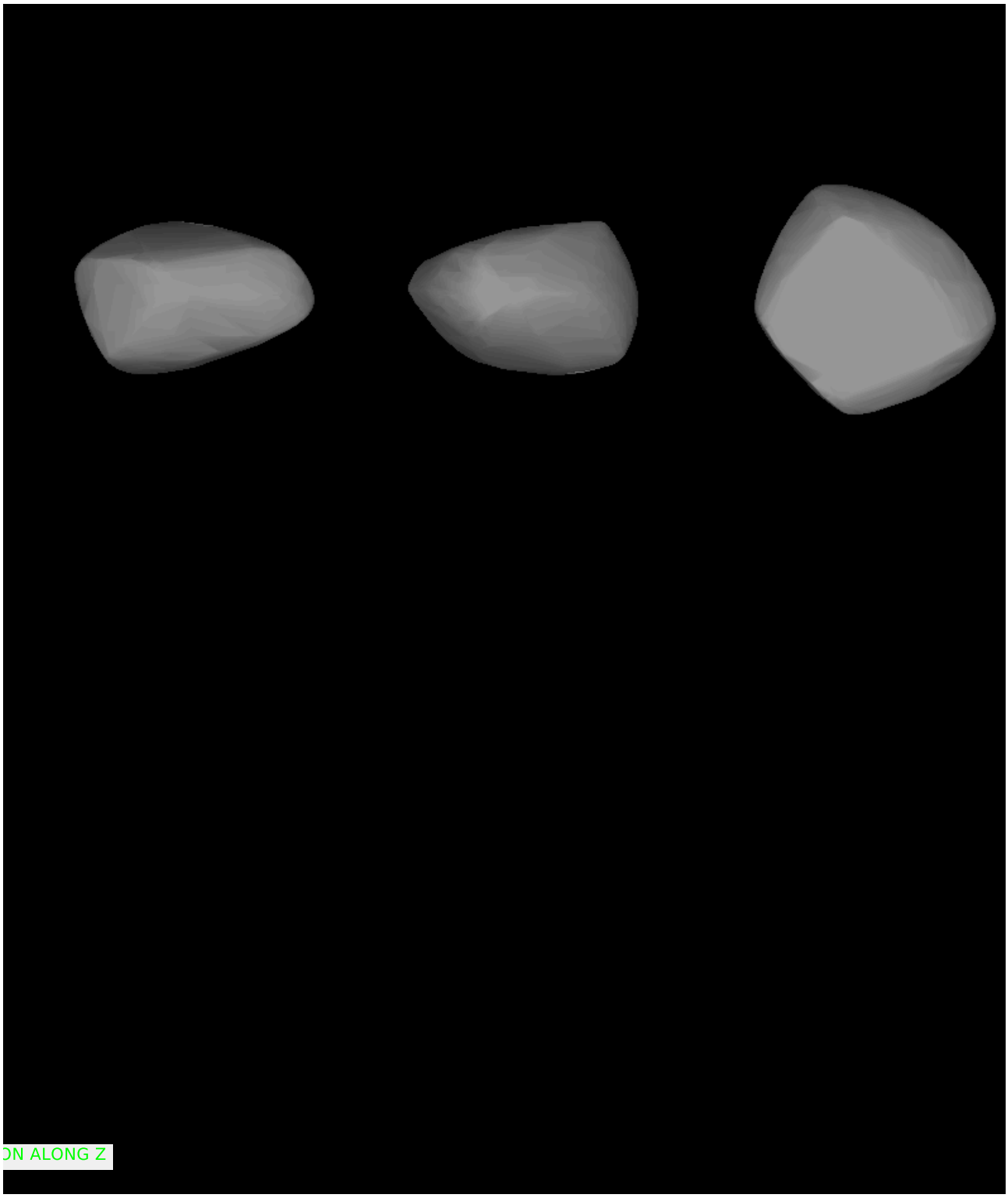

Figure 6: S1. Asteroid shape 2.

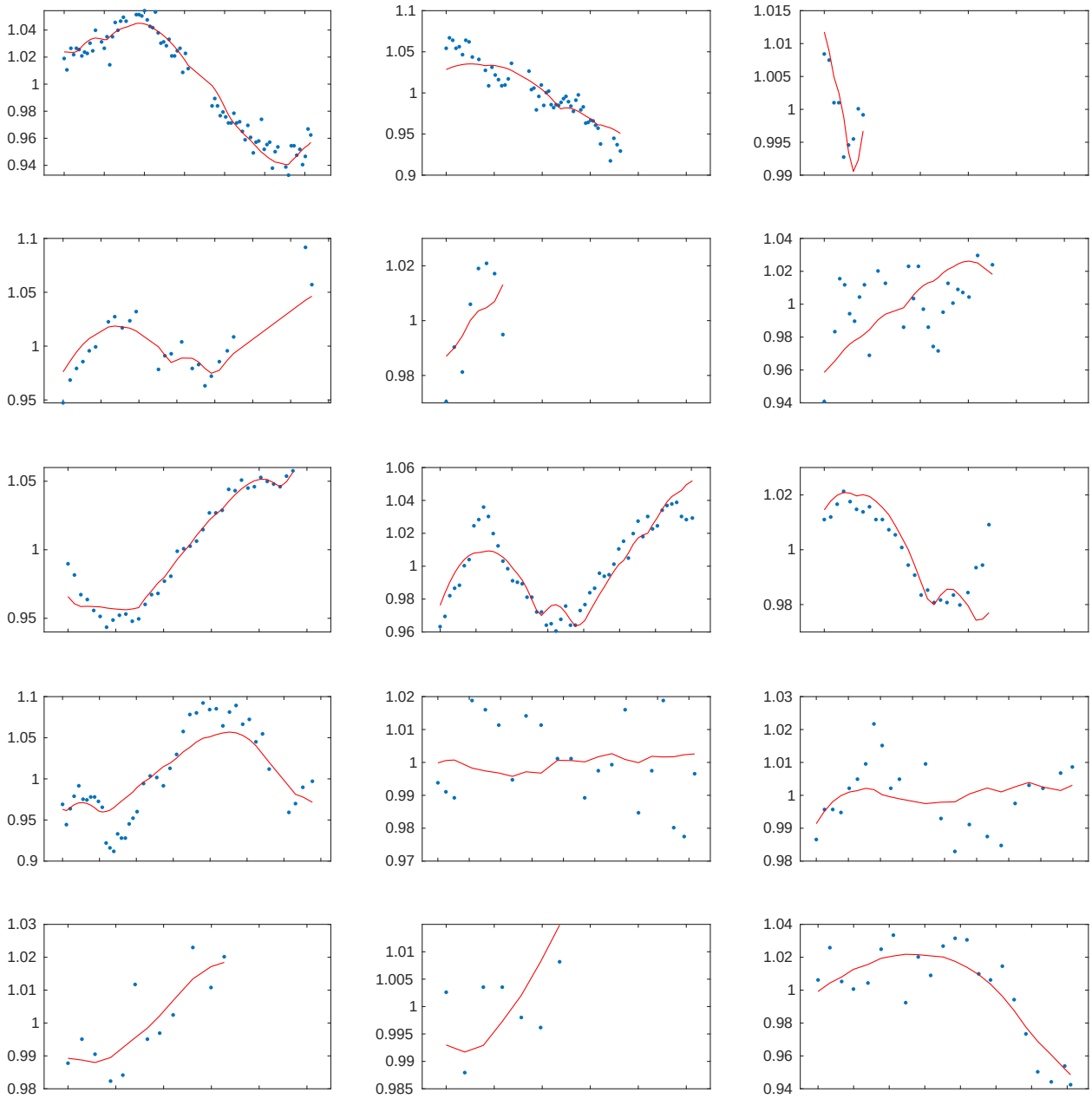

Figure 7: S1. Observed lightcurves (blue points) vs. those synthetic (red lines). Part 1.

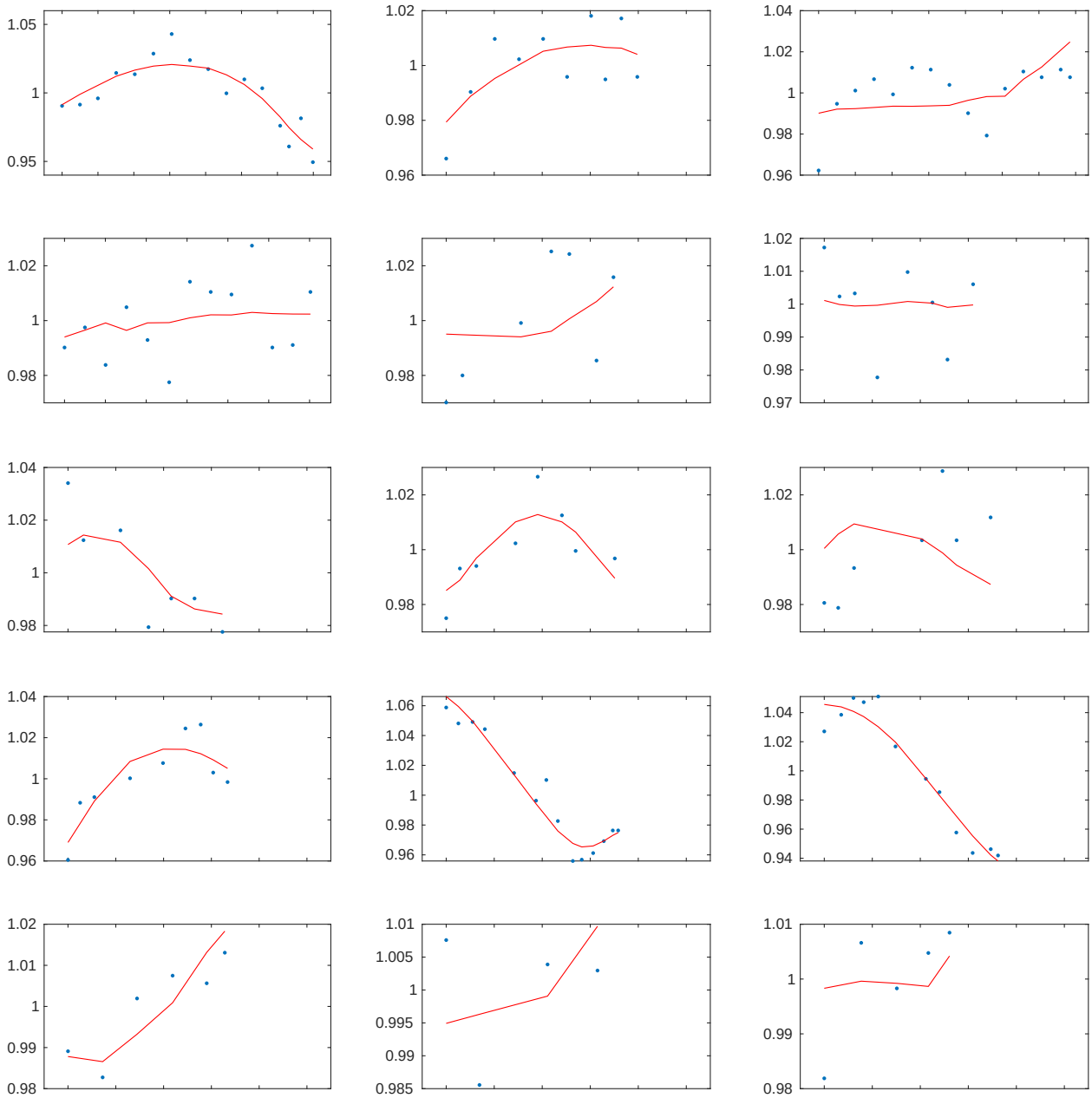

Figure 8: S1. Observed lightcurves (blue points) vs. those synthetic (red lines). Part 2.

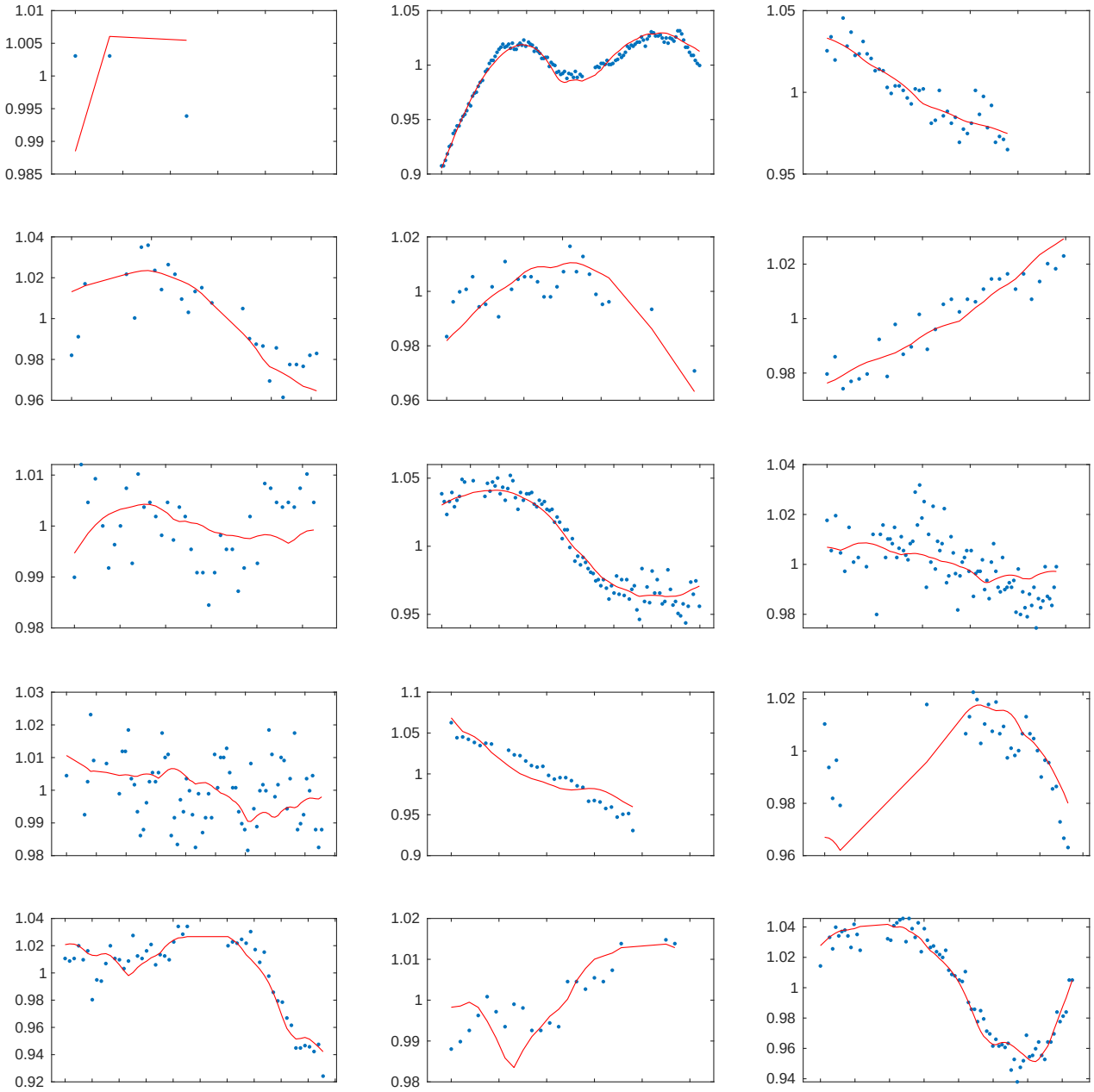

Figure 9: S1. Observed lightcurves (blue points) vs. those synthetic (red lines). Part 3.

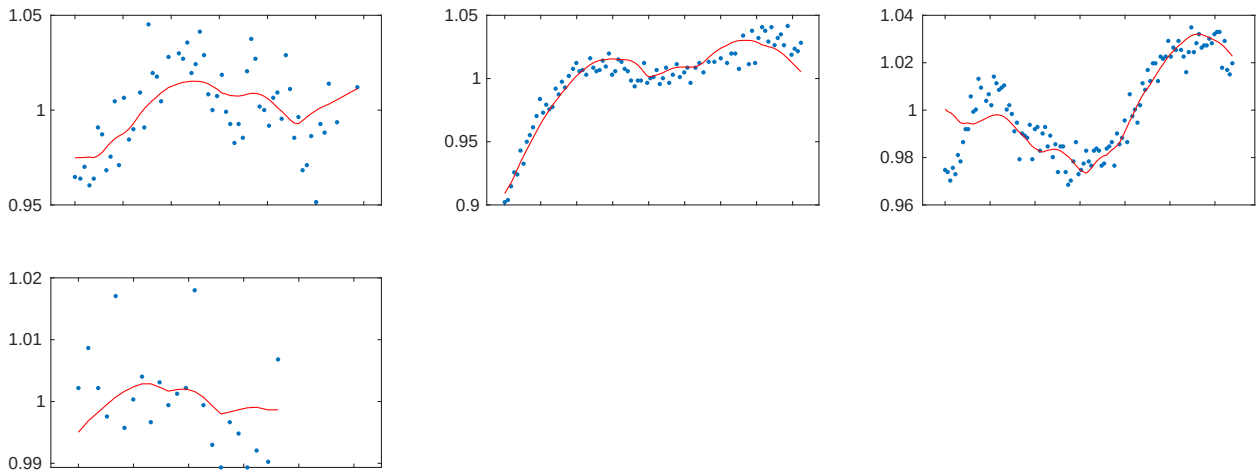

Figure 10: S1. Observed lightcurves (blue points) vs. those synthetic (red lines). Part 4.

Figure 11: S2. Asteroid shape 1.

Figure 12: S2. Asteroid shape 2.

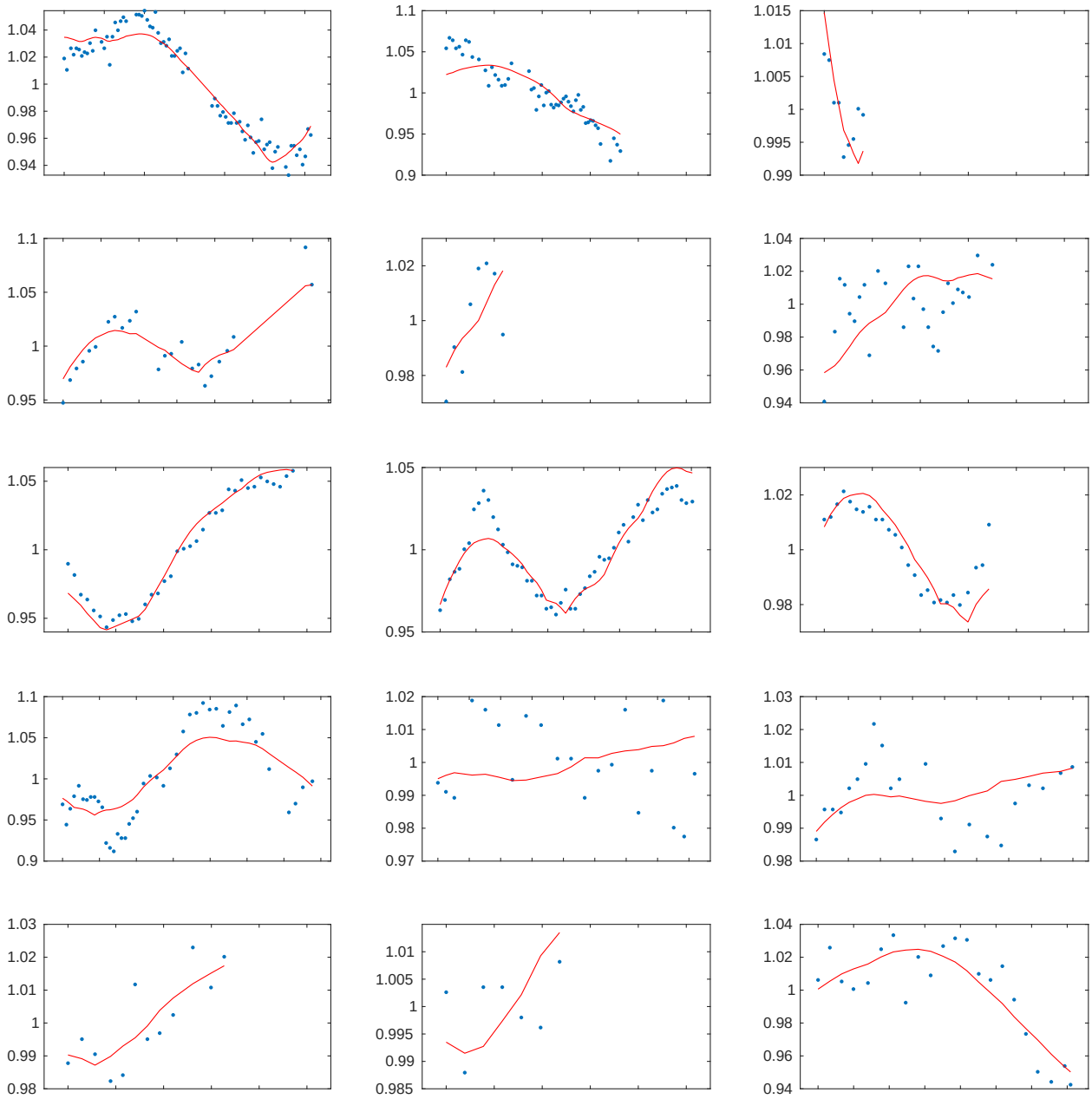

Figure 13: S2. Observed lightcurves (blue points) vs. those synthetic (red lines). Part 1.

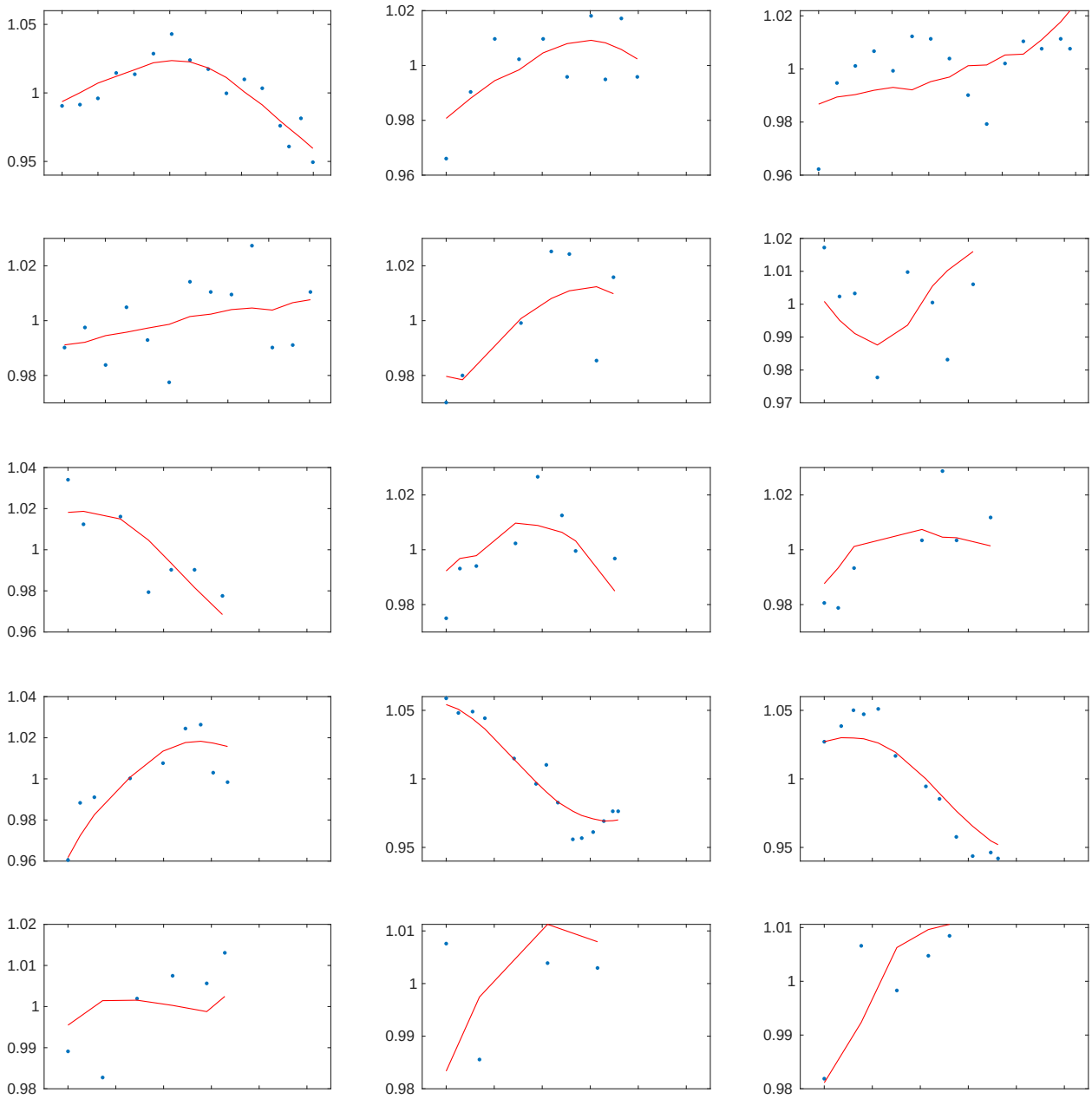

Figure 14: S2. Observed lightcurves (blue points) vs. those synthetic (red lines). Part 2.

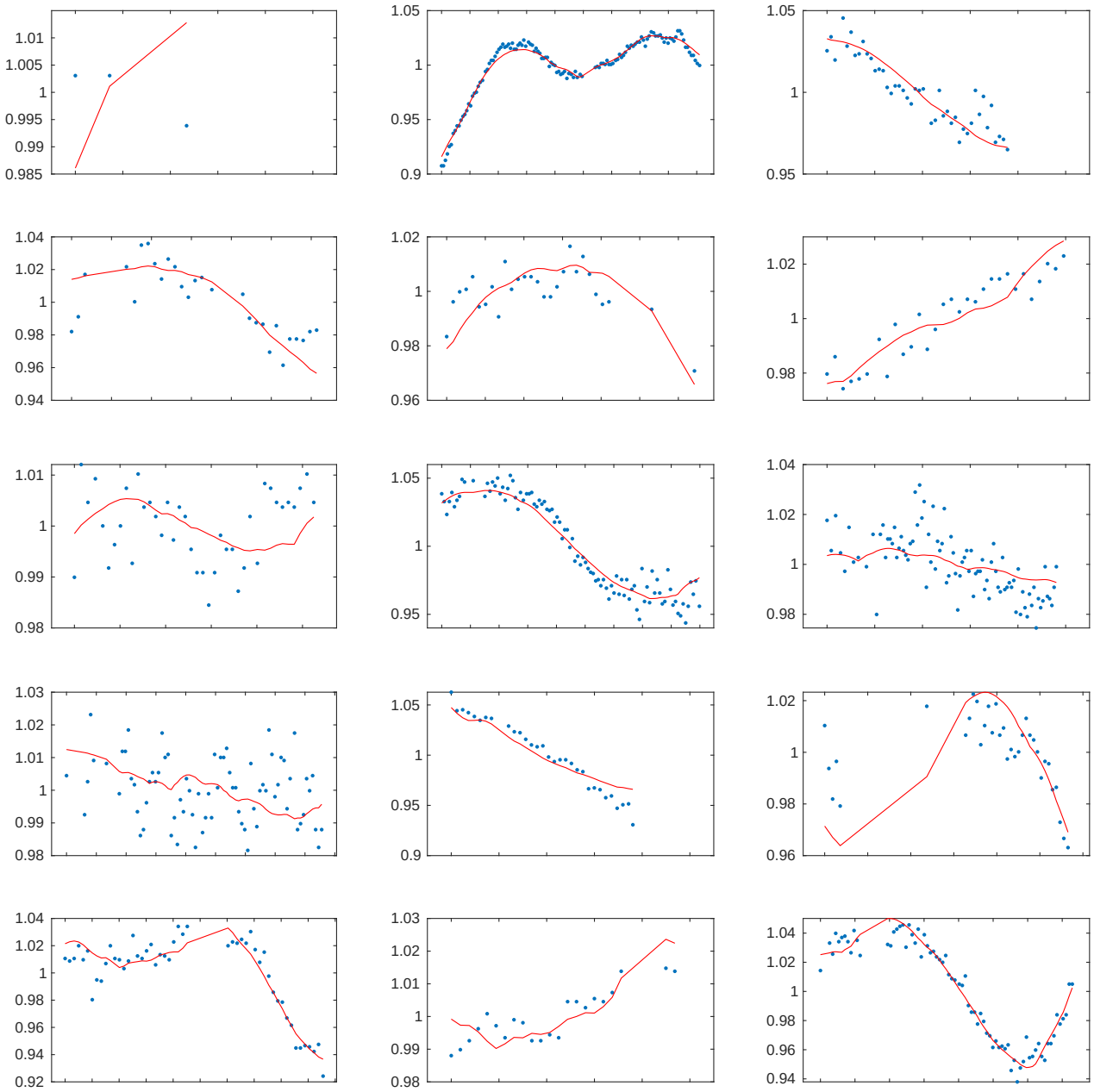

Figure 15: S2. Observed lightcurves (blue points) vs. those synthetic (red lines). Part 3.

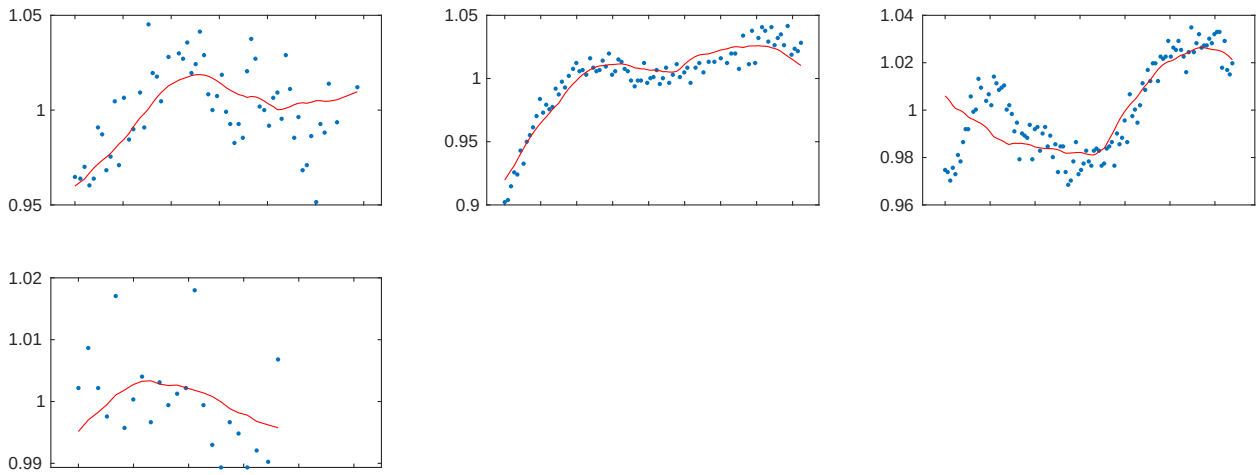

Figure 16: S2. Observed lightcurves (blue points) vs. those synthetic (red lines). Part 4.